

GEOMETRIC PROPERTIES OF LEPTODERMOUS DISTRIBUTIONS WITH APPLICATIONS TO NUCLEI

WILLIAM D. MYERS

Lawrence Berkeley Laboratory, University of California, Berkeley, California 94720†

Received 9 January 1973

Abstract: Relationships between geometrical properties of leptodermous distributions are employed in the interpretation of experimentally determined nuclear density distributions and optical-model potential wells. It is found that nuclear sizes imply a density for neutral symmetric nuclear matter corresponding to $r_0 = 1.16$ fm ($k_r = 1.31$ fm⁻¹) and that the densities and potentials can be related to each other by means of a saturating two-body interaction.

1. Introduction

Many different algebraic functions have been employed from time to time to represent nuclear density distributions and potential wells¹). The parameters occurring in these functions (chosen to best reproduce some experimental result) are generally without special physical significance. Consequently, various “abstract” quantities have been employed in an attempt to characterize these functions in ways independent of the particular functions used. Quantities of this type, such as the half-value radius or the root-mean-square radius, have been chosen because there is either theoretical expectation or empirical observation that they are nearly model independent.

Strictly speaking, none of the abstract quantities commonly employed to characterize the size of the nuclear density distribution or potential well are expected, on the basis of nuclear saturation, to be proportional to $A^{\frac{1}{3}}$. When the ratio of these quantities to $A^{\frac{1}{3}}$ is referred to as the “nuclear radius constant” or simply r_0 , a great deal of confusion is created. This confusion, which permeates the nuclear physics literature, can be easily avoided if the characterization scheme outlined in sect. 2 is used.

2. Geometrical preliminaries

2.1. LEPTODERMOUS†† DISTRIBUTIONS

The discussion of radial geometric properties of nuclei (here assumed to be spherical) is most easily carried out in terms of the quantities:

† Work performed under the auspices of the US Atomic Energy Commission.

†† Leptodermous – having a thin skin. This term has been employed by Swiatecki and co-workers^{2,5}) for the depiction of distributions which are essentially homogeneous except at the surface. Its application implies that $b/R \ll 1$ and that all deviations from bulk behavior are confined to a relatively thin surface region.

- C , the "central radius",
 R , the "equivalent sharp radius",
 Q , the "equivalent rms radius" and
 b , the "surface width".
- (1)

It is essential for the clarity of the following discussions that the definitions of these quantities and the relations between them be precisely understood.

The central radius C and the surface width b are the integral counter-parts of the punctual quantities:

$$\begin{aligned}
 R_{\frac{1}{2}}, & \text{ the half-value radius, and} \\
 t_{10-90}, & \text{ the 10-90 \% distance.}
 \end{aligned}$$

(2)

They are defined in terms of linear moments (as opposed to spherical moments) of the derivative of the normalized [$f(0) = 1$] distribution function. If (as illustrated in fig. 1) $f(r)$ is the distribution of interest, then

$$\begin{aligned}
 C &= \int_0^{\infty} g(r) r dr, \\
 b^2 &= \int_0^{\infty} g(r) (r - C)^2 dr, \\
 \int_0^{\infty} g(r) dr &= 1,
 \end{aligned}$$

(3)

where the surface distribution function $g(r)$ is defined by the expression

$$g(r) = -df(r)/dr. \quad (4)$$

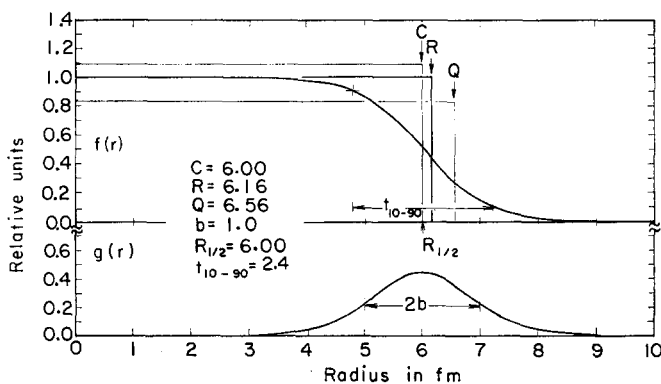


Fig. 1. The normalized, spherically symmetric, leptodermous distribution $f(r)$ and the corresponding surface distribution function $g(r)$ are plotted against the radial distance r . The values of $R_{\frac{1}{2}}$ and t_{10-90} are given for this distribution in addition to the values of C , R , Q , and b whose use is advocated here. Sharp density distributions having the same volume integral as $f(r)$ and radii equal to C , R , and Q have also been drawn in for the purpose of demonstrating the geometrical importance of R .

The quantities C and b are the first two moments of the distribution $g(r)$. In a similar way additional information about the surface is available from higher moments such as the skewness and the kurtosis of this distribution, which can be obtained from Γ_3 and Γ_4 , respectively, where

$$\Gamma_n = \int_0^\infty g(r)(r-C)^n dr. \quad (5)$$

This approach to the characterization of leptodermous distributions has been brought to a high degree of refinement by Süssman²⁾, and the notation used here closely follows his.

For the commonly used Fermi distribution function

$$f(r) = 1/\{1 + \exp[(r-c)/z]\}, \quad (6)$$

the quantities C , $R_{\frac{1}{2}}$, b , and t_{10-90} are related to c and z (for $e^{-c/z} \ll 1$) by the expressions

$$\begin{aligned} C &= R_{\frac{1}{2}} = c, \\ b &= (\pi/\sqrt{3})z, \\ t_{10-90} &= (2 \ln 9)z. \end{aligned} \quad (7)$$

The next quantity of interest is the equivalent sharp radius R . It is defined here as the radius of a uniform sharp distribution having the same value in the bulk and the same volume integral as $f(r)$, i.e.,

$$\frac{4}{3}\pi R^3 f(\text{bulk}) = 4\pi \int_0^\infty f(r)r^2 dr. \quad (8)$$

For smooth leptodermous distributions (such as a Fermi distribution) the bulk value corresponds very closely to the central value and to this approximation $f(0)$ can be substituted for $f(\text{bulk})$ in eq. (8). Of course, for distributions that are leptodermous except for some smooth oscillations in the interior (for example, nuclear density distributions found in shell model or Hartree-Fock calculations) the punctual value $f(0)$ is clearly inadequate for the definition of R and some suitable average bulk value must be employed.

The final quantity of interest is the equivalent root-mean-square radius Q , which is defined by the expression

$$Q^2 = \frac{5}{3}\langle r^2 \rangle, \quad (9)$$

where

$$\langle r^n \rangle = \frac{\int_0^\infty r^n f(r)r^2 dr}{\int_0^\infty f(r)r^2 dr}. \quad (10)$$

The quantity Q is the special case for $k = 2$ of the quantity

$$R_k = [\frac{1}{3}(k+3)\langle r^k \rangle]^{1/k}, \quad (11)$$

of Ford and Wills³).

Of the three quantities C , R , and Q , the quantity of fundamental geometric importance is the equivalent sharp radius R . A sharp sphere having this radius is in a basic sense representative of the distribution $f(r)$. If the uniform central density of such a sharp sphere is set equal to the bulk value of $f(r)$, as defined in connection with eq. (8), then this sphere has the same volume integral as $f(r)$ and it differs from $f(r)$ *only in the surface region* (namely in the degree of diffuseness). The quantity C is mainly of interest because $R_{\frac{1}{2}} = C$ for the symmetric surface functions (such as Fermi distributions) often employed to characterize nuclear densities and potential wells. The equivalent rms radius Q is of interest since it is expected that this is the property of the distribution that is measured in some experiments^{3,4}). As can be seen in fig. 1, sharp spheres with the same volume integral as $f(r)$ having the radii C or Q grossly misrepresent the appearance of the function $f(r)$, since they substantially differ from it over the bulk region.

Süssmann has given exact expressions relating C and Q to R in terms of b and higher-order moments of the surface²). However, the following approximate expressions suffice for most applications, and serve as simple reminders of the relationships of these quantities to each other:

$$\begin{aligned} C &= R[1 - \beta^2 + \dots], \\ Q &= R[1 + \frac{5}{2}\beta^2 + \dots], \end{aligned} \quad (12)$$

where

$$\beta = b/R. \quad (13)$$

The range of applicability of these simple relationships can be seen in fig. 2 where the ratios C/R and Q/R have been plotted against β^2 for a Fermi distribution. The solid straight lines correspond to the approximate predictions of eqs. (12) and the dashed lines to the actual values. At the top of the figure the approximate nuclear mass number is plotted corresponding to the assumption that nuclear density distributions can be represented by Fermi distributions with $R = 1.16 A^{\frac{1}{3}}$ and $b = 1.0$. We can see from this scale that eqs. (12) are expected to be accurate to within 1 % for C and 5 % for Q all the way down to mass number $A = 9$. They are considerably more accurate over the bulk of the periodic table.

The relationship of C and Q to the more fundamental quantity R can be seen by referring back to fig. 1. In this figure a Fermi distribution with $R_{\frac{1}{2}} = 6.00$ fm and $t_{10-90} = 2.4$ fm has been chosen to illustrate the geometric principles just described. The surface distribution function $g(r)$ has its first moment C – identical to $R_{\frac{1}{2}}$ in this case – and second moment b indicated in the figure. The radius R of the sharp sphere representing the function $f(r)$ is shown, as is the radial location corresponding to the value of Q . In any discussion of the geometric properties of this system, interest should

focus on the equivalent sharp sphere whose radius is R and on the value of the surface thickness b . Other geometric properties that may be of interest can then be obtained from eqs. (12) or similar expressions.

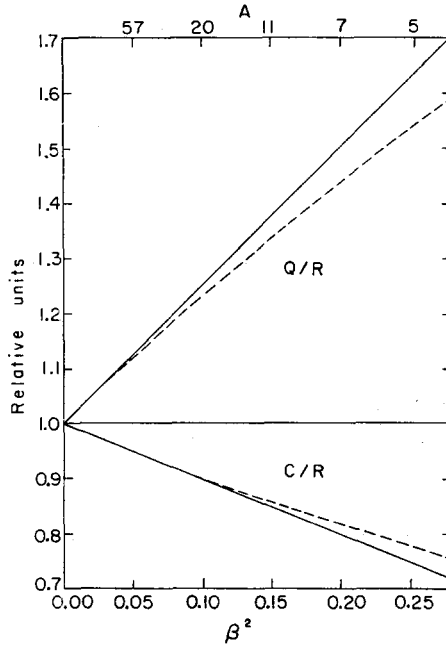


Fig. 2. The dashed lines plotted against β^2 represent the quantities Q/R and C/R for a Fermi function, and the solid lines represent the predictions of eqs. (12). The upper scale gives the corresponding nuclear mass number.

2.2. DISTRIBUTIONS RELATED BY CONVOLUTION

There is a second distinct class of geometrical relationships in addition to the ones just discussed that is also of considerable interest. These relationships connect the geometrical properties of one leptodermous distribution to the corresponding properties of a second distribution which is obtained from the first by folding in a function of short range. One example is a nuclear charge distribution obtained by folding the proton charge distribution into the assumed spatial distribution of the protons. Another example is a single-particle or optical-model potential well obtained by folding a two-body interaction into the nuclear density distribution.

If the first distribution is $f_1(\bar{r}_1)$ and the folding (or convolution) function is $f_c(\bar{r}_{12})$, then the second distribution $f_2(\bar{r}_2)$ is defined by

$$f_2(\bar{r}_2) = \int d\bar{r}_1 f_1(\bar{r}_1) f_c(\bar{r}_{12}). \quad (14)$$

Probably the best-known expression relating the geometric properties of f_1 and f_2 is

$$\langle r^2 \rangle_2 = \langle r^2 \rangle_1 + \langle r^2 \rangle_c. \quad (15)$$

Substitution of eq. (9), which relates Q and $\langle r^2 \rangle$, into eq. (15) results in the expression

$$Q_2^2 = Q_1^2 + \frac{5}{3} \langle r^2 \rangle_c. \quad (16)$$

Another useful relationship that can be easily established with the aid of eqs. (12) and (19) is

$$b_2^2 = b_1^2 + b_c^2 + \text{terms of order } \beta^2, \quad (17)$$

where the "width" b_c of the folding function has the special definition

$$b_c^2 = \frac{1}{3} \langle r^2 \rangle_c. \quad (18)$$

Since the expression relating the values of Q_1 and Q_2 shows that $Q_2 > Q_1$ in correspondence with one's intuition that f_2 should somehow be bigger than f_1 , it may come as a surprise that the equivalent sharp radii R_1 and R_2 are equal for leptodermous distributions where $\beta \ll 1$.

This result follows directly from the fact that the volume integral of f_2 is equal to the product of the volume integrals of f_1 and f_c . The easiest way to establish the relationship between R_1 and R_2 is to consider a normalized leptodermous function f_1 (where $f_1(\text{bulk}) = 1$) and a folding function f_c whose volume integral is unity. In such a case f_2 will also be normalized ($f_2(\text{bulk}) = 1$) and have the same volume integral as f_1 . Then from the definition of R in eq. (8) it is easy to see that

$$R_1 = R_2, \quad \text{when } \beta \ll 1. \quad (19)$$

Eqs. (12), (13), (17), and (19) can be combined to give the following set of relations between the geometric properties of f_1 and f_2 , which hold for $\beta \ll 1$:

$$\begin{aligned} C_2 &= C_1(1 - \beta_c^2 + \dots), \\ R_2 &= R_1, \\ Q_2 &= Q_1(1 + \frac{5}{3}\beta_c^2 + \dots). \end{aligned} \quad (20)$$

These expressions show that when a short-range function is folded into a leptodermous distribution, another distribution is obtained that has a larger equivalent rms radius Q , an identical equivalent sharp radius R , and a central radius C that is smaller than the values of the corresponding quantities for the initial distribution.

3. Nuclear density distributions

3.1. INTERPRETATION OF EXPERIMENTS

The geometrical considerations of sect. 2, which apply to any leptodermous distribution, are especially useful in the interpretation of experimental measurements of nuclear density distributions. They permit one to extract from these experiments an estimate of the equilibrium density ρ_0 of neutral (all electromagnetic effects ignored) symmetric ($\rho_n = \rho_z$) nuclear matter. The quantity r_0 (a fundamental constant of nuclear physics) can then be calculated from the relationship

$$\rho_0 = \left(\frac{4}{3}\pi r_0^3\right)^{-1}. \quad (21)$$

If nuclear matter were incompressible and nuclei had bulk neutron and proton densities in the ratio N/Z , then the equivalent sharp radii R_n and R_z of the neutron and proton distributions would be equal and proportional to $A^{1/3}$ with a proportionality constant equal to r_0 , i.e.,

$$R_n = R_z = r_0 A^{1/3}. \quad (22)$$

Of course, this simple relationship is not expected to hold exactly because nuclear matter is not completely incompressible. Small deviations are expected – for example, see refs. ⁵⁻⁹ – because the surface energy tends to squeeze the nucleus to a smaller radius, and both the Coulomb energy and the loss of cohesion due to excess neutrons cause the nucleus to dilate to a larger radius. Since the relative importance of these effects varies through the periodic table, some nuclei are smaller and some larger than is predicted by eq. (22). Another effect of the excess neutrons is the creation of a neutron skin.

Consequently, not only does the average radius R_ρ differ from eq. (22), but the separate neutron and proton radii (R_n and R_z) differ from R_ρ and from each other. The expressions relating these quantities are

$$\begin{aligned} R_\rho &= (NR_n + ZR_z)/A, & R_n &= R_\rho + (Z/A)t, \\ t &= R_n - R_z, & R_z &= R_\rho - (N/A)t, \end{aligned} \quad (23)$$

where the effective sharp radius of the matter distribution R_ρ is the weighted average of R_n and R_z and t is the neutron skin thickness. [See ref. ⁶.]

It should be noted that even if nuclear matter were incompressible and R_n and R_z were strictly proportional to $A^{1/3}$, the quantities C and Q would not [as can be seen in eqs. (12)] be simply proportional to $A^{1/3}$. In spite of this, attempts are often made to establish such relationships. Exceptions to this erroneous approach are to be found in a number of places such as refs. ^{1, 10}) where Elton makes use of expressions similar to eqs. (12) (but specialized to Fermi distributions and taken to higher order) to relate C and Q to the more fundamental quantity R .

Fig. 3 shows what happens when the ratio of C or Q to $A^{1/3}$ is plotted against A for nuclei throughout the periodic table. The data points, which are all from ref. ¹), are represented by circles when they are based on Q -values from μ -mesic atom experiments and by triangles when they are based on C (or R_\pm) values from electron scattering. The reason for listing the C -values for electron scattering is that this quantity and the quantity b are the properties of the nuclear charge distribution that are determined (to lowest order in β^2) by the experiments ¹¹). Similarly, the quantity Q is plotted for the μ -mesic atom experiments because it is the one actually determined ³). While the $Q/A^{1/3}$ values are not exactly constant they do seem to tend to an asymptotic value of about 1.2 fm, and the $C/A^{1/3}$ values seem to tend to approximately 1.1 fm. The numbers obtained in this way are often erroneously assumed to correspond to the fundamental constant r_0 defined in eq. (21).

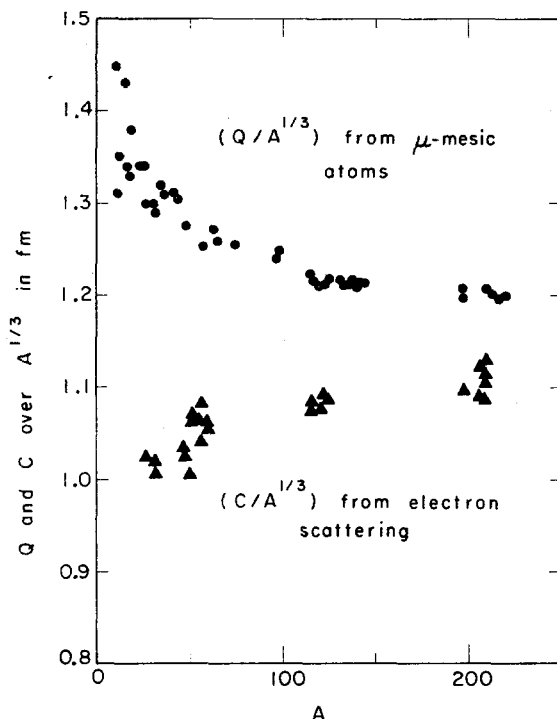


Fig. 3. A plot of experimental values of $Q/A^{1/3}$ from μ -mesic atoms and $C/A^{1/3}$ from electron scattering against mass number A for nuclei throughout the periodic table¹⁾.

That there is no discrepancy between the two different types of measurements is easily seen in fig. 4. If R_z were nearly proportional to $A^{1/3}$ then eqs. (12) could be re-written in the form

$$\begin{aligned} C_z/A^{1/3} &\approx a[1 - (b/a)^2 A^{-2/3} + \dots], \\ R_z/A^{1/3} &\approx a, \\ Q_z/A^{1/3} &\approx a[1 + \frac{5}{2}(b/a)^2 A^{-2/3} + \dots]. \end{aligned} \quad (24)$$

These expressions lead us to expect straight lines (in the limit of $A^{-2/3} \ll 1$) when the experimental ratios of C and Q to $A^{1/3}$ are plotted against $A^{-2/3}$. In fig. 4 we see that this expectation is fulfilled and that the data, except for the lightest nuclei, are consistent with straight lines having a common intercept at

$$a = 1.128 \text{ fm}, \quad (25)$$

and slopes corresponding to

$$b = 1 \text{ fm}. \quad (26)$$

According to eqs. (7), this implies a value for t_{10-90} of 2.4 fm for a Fermi distribu-

tion. In this figure the solid squares represent values of $R_z/A^{1/3}$ determined from the C_z and Q_z values by inverting eqs. (12). The figure shows that this quantity is in fact nearly independent of nuclear size.

If nuclear matter were strictly incompressible and if the equivalent sharp radii of the neutrons and protons (R_n and R_z) were identical, then the fundamental constant r_0 would have the same value as the proportionality constant (1.128 fm) determined above. The actual, more complex, relationship between these quantities has been investigated with the droplet model of nuclei which includes such important effects as compressibility and the influence of the neutron excess on the creation of a neutron skin ^{5, 6}).

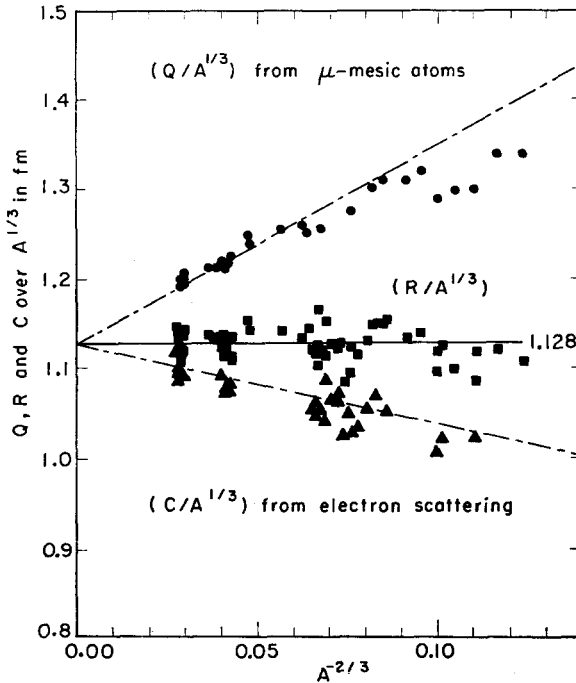


Fig. 4. The same experimental values of $Q/A^{1/3}$ and $C/A^{1/3}$ as were used in fig. 3 are plotted here against $A^{-2/3}$. The values of $R/A^{1/3}$ for these experimental points are also plotted and are seen to scatter about the solid horizontal line at 1.128 fm. The corresponding predictions for $Q/A^{1/3}$ and $C/A^{1/3}$ are given as dot-dashed lines.

3.2. NUCLEAR RADIUS CONSTANT

Fig. 5 gives the results of a droplet model calculation performed for the purpose of showing the relationship between r_0 and the experimentally determined proportionality constant that relates R_z (the equivalent sharp radius of the proton distribution) to $A^{1/3}$. The grey band centered at 1.128 fm is meant to represent the experimental results from the previous figure (notice the greatly expanded scale). When a droplet model calculation is carried out for nuclei throughout the periodic table for a system whose

nuclear radius constant r_0 is 1.163 fm [recall that r_0 is related to ρ_0 , the density of $N = Z$ nuclear matter, by eq. (21)], the value of the ratio $R_\rho/A^{1/3}$ is given by the dashed line. For most nuclei this line lies below that at $r_0 = 1.163$ fm, because these nuclei are being squeezed by the surface tension. As one proceeds through the periodic table this squeezing (which is strongest for the lightest nuclei) is gradually offset by the Coulomb dilation so that above $A \approx 250$ the nuclei are larger than $r_0 A^{1/3}$. (The increase in this quantity for small A values is a geometrical rather than a physical effect, brought about by the fact that light nuclei are no longer leptodermous.)

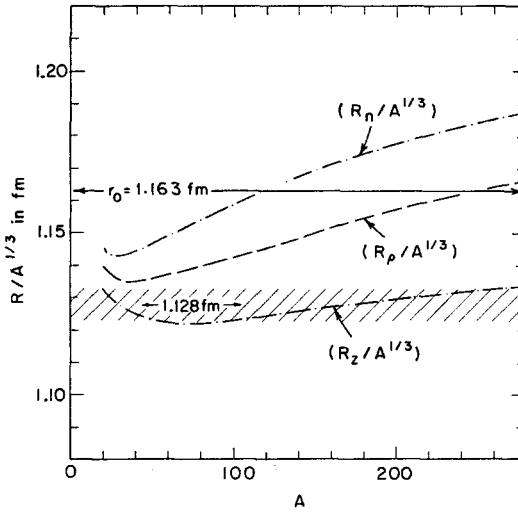


Fig. 5. The dot-dashed lines represent the results of droplet model calculations for $R_z/A^{1/3}$ and $R_n/A^{1/3}$ plotted against A for nuclei along β -stability. Their weighted average $R_\rho/A^{1/3}$ is plotted as a dashed line and the corresponding value of r_0 is indicated by the solid horizontal line at 1.163 fm. The striped region corresponds to the approximate location of the experimental values of $R_z/A^{1/3}$.

The dot-dashed lines showing the separate neutron and proton radii, R_n and R_z , show the same trend with A as the total matter radius R_ρ . In addition they spread further and further apart as the neutron skin thickness grows due to the increasing neutron excess with increasing values of A . The growth of this neutron skin (whose thickness is about 0.25 fm at $A = 200$) reduces the increase in $R_z/A^{1/3}$ with the consequence that this ratio is nearly constant throughout the periodic table. The value of $r_0 = 1.163$ fm was chosen for this calculation so the experimental and calculated radii for the proton distributions would agree.

We can conclude that the nuclear radius constant of standard nuclear matter can be inferred with considerable accuracy from the experimental results, which only determine the radius of the proton distribution R_z , and that it has the approximate value

$$r_0 = 1.16 \text{ fm}, \quad (27)$$

which corresponds to a value for k_f of 1.31 fm^{-1} . An uncertainty of perhaps $\pm 1\frac{1}{2}\%$ should be assigned to this number because of the scatter in the experimental points and because there is some model dependence in the way it is obtained. This is the value of r_0 that should be employed in nuclear matter calculations rather than the unwarranted choice of values like 1.1 fm or 1.2 fm that we discussed earlier in connection with fig. 3.

The equivalent sharp radii of the proton distributions are given approximately by $A^{\frac{1}{3}}$ times the proportionality constant in eq. (25), 1.128 fm, or more precisely by performing the appropriate droplet model calculation ⁶⁾ with the value of r_0 , 1.16 fm, given above. Once R is known then eqs. (12) can be used to make the simple geometrical corrections necessary to determine C and Q for comparison with experiment.

3.3. INFLUENCE OF PROTON CHARGE DISTRIBUTION

Another question that sometimes arises in the interpretation of experimental measurements of the nuclear charge distribution is whether or not the proton charge distribution should be unfolded in order to obtain the distribution of the protons themselves. This is an important distinction, since the bulk density of the protons is the appropriate quantity to consider in relating the experiments to a value for the constant r_0 . Fortunately, the value of the equivalent sharp radius R_z (which we have shown is the only geometrical quantity of interest in determining r_0) has been shown in eq. (19) to be identical for the proton distribution and the charge distribution. Earlier authors' concern over unfolding the charge distribution to obtain the actual proton distribution was due to the fact that the quantities C_z or Q_z were being erroneously employed in the determination of r_0 .

4. Optical-model potential wells

The geometrical relationships given earlier, and employed in sect. 3 for the interpretation of nuclear density distributions, apply equally well to optical-model potential wells. Indeed, the Woods-Saxon functional form of optical-model wells is the same Fermi distribution as is used to describe nuclear densities. As regards geometrical properties the main difference between the optical-model wells and the density distributions is that there is no reason to expect – even under the assumption of incompressibility – the equivalent sharp radius of the potential R_v to be proportional to $A^{\frac{1}{3}}$.

4.1. INTERPRETATION OF EXPERIMENTS

Many authors, unsatisfied with simply fitting potential well parameters to experiment, have cast about for some plausible scheme for correlating the results obtained for different nuclei. The procedures that have come into common use, such as “fixed geometry fits” and various ways of deriving the potentials by folding an interaction into the density, all have serious deficiencies. The problems that arise when these methods are employed will be discussed below in connection with fig. 6.

The three separate sections of fig. 6 have been collected together because of their similarity, and to facilitate comparisons between one section and another as the discussion progresses. After the features common to all three sections have been explained each separate section will be discussed in turn.

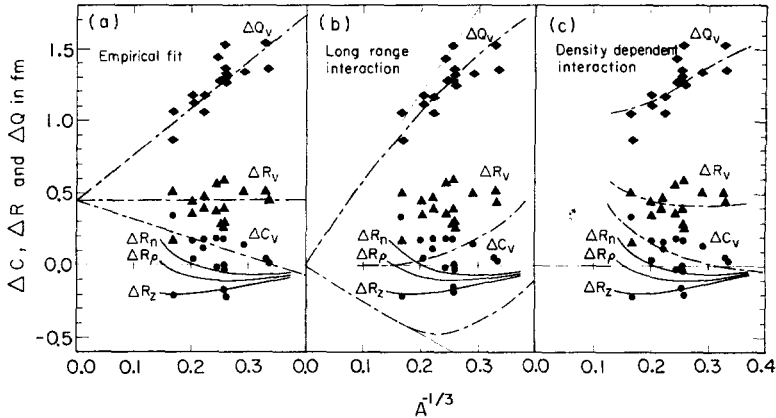


Fig. 6. The differences (signified by Δ) between the Q_v , R_v , and C_v values of experimental optical-model potentials^{12,13} and reference values equal to $1.16 A^{1/3}$ fm are plotted against $A^{-1/3}$. Similarly the solid lines at the bottom of each section represent droplet model predictions for the various matter radii. The dot-dashed lines represent three different ways of correlating the experimental information on the potential wells: (a) an empirical fit, (b) a fit obtained by folding a non-saturating force into empirical density distributions, and (c) a fit obtained by folding a saturating force into the droplet model density distributions.

The experimental data consist of Woods-Saxon well parameters given in refs.^{12,13} for optical-model fits to 40–60 MeV proton scattering on nuclei throughout the periodic table. Eqs. (7), (12) and (13) have been used to convert these parameters to values of Q_v , R_v and C_v for each of the potential wells. (The subscript v means that these quantities refer to geometrical properties of the potential.) Then the quantity $1.16 A^{1/3}$ fm was subtracted from each of these numbers for the sole purpose of displaying, on an expanded scale, the relations between the different quantities.

The values actually plotted versus $A^{-1/3}$ in each section of the figure are ΔQ_v (as diamonds), ΔR_v (as triangles), and ΔC_v (as circular dots), where

$$\begin{aligned}\Delta Q_v &= Q_v - 1.16 A^{1/3}, \\ \Delta R_v &= R_v - 1.16 A^{1/3}, \\ \Delta C_v &= C_v - 1.16 A^{1/3}.\end{aligned}\tag{28}$$

The heavy solid lines near the bottom of each section represent the values of ΔR_ρ , ΔR_n and ΔR_z obtained from a droplet model calculation of these quantities (discussed earlier in connection with fig. 5) that is fitted to the experimental values of R_z . Since these lines represent the various nuclear density distributions and the experimental

points represent various properties of the potential wells we might expect to learn a great deal from these figures about the relationships between them.

One of the first things one notices in fig. 6 is that R_v is greater than R_p by an almost constant amount throughout the periodic table. In fact, very close correspondence can be seen in fig. 6a between the experimental points and the dot-dashed lines that correspond to

$$\begin{aligned} R_v &= 1.16A^{\frac{1}{3}} + 0.45 \text{ fm}, \\ b_v &= 1.3 \text{ fm}. \end{aligned} \quad (29)$$

In the "fixed-geometry fits" commonly employed for the interpretation of optical-model data, the half-value radius $R_{\frac{1}{2}}$ is generally assumed to be proportional to $A^{\frac{1}{3}}$, and some suitable value is chosen for the proportionality constant so as to best reproduce data throughout the periodic table. The choice of the quantity $R_{\frac{1}{2}}$ for a parametrization of this kind is puzzling, since we showed earlier that a sharp sphere with the radius C_v does not serve to represent the corresponding distribution (recall that $R_{\frac{1}{2}} = C$ for Woods-Saxon wells.) Moreover, there is no physical basis for assuming such proportionality for the potential well, even for the more fundamental quantity R_v . The main reason for constraining the fits in this way has been to force an apparent reduction in the uncertainty of the determination of the real and imaginary potential well depths. The trends in these quantities with increasing mass number and neutron excess are then considered to be significant, and physical interpretation of the results is sometimes attempted. It should, however, be clear by now that this whole procedure is questionable [see ref. 4) for other comments along this line], since the unjustified nature of the constraints probably introduces spurious trends into other quantities of interest.

4.2. POTENTIALS OBTAINED BY FOLDING

Other authors, unsatisfied with simply fitting well parameters to experiment or using empirical relations like eq. (29) to correlate their data, have employed optical potentials obtained from the nuclear density distributions by folding in a simple two-body interaction. To appreciate some of the problems that can arise when this is done it is necessary to recall the relations between the geometrical properties of such distributions as given in eqs. (20). These equations immediately bring one difficulty to our attention, since they show that R_v must equal R_p , in direct disagreement with the experimental results shown in fig. 6.

This discrepancy manifests itself in different ways in the two distinctly different approaches that have been taken. Some authors take the density distribution from electron scattering as given and fold in a rather long-range force to generate an optical potential that fits the experimental data. This method is considered in refs. ^{14, 15}) along with a number of others. It results in a more diffuse potential than would be obtained in an optical-model fit, but one which has approximately the same value for Q_v . [It has been found empirically that different potentials having the same volume

integral and the same equivalent rms radius Q_v give approximately the same predictions.] The values of the geometrical parameters R_v and b_v of the resulting potential differ substantially from the values that would be obtained for a Woods-Saxon well fitted directly to experiment. Other authors allow the density to vary in the fitting process and obtain potentials very similar to those found by fitting Woods-Saxon wells ⁴). However, the geometrical parameters of the density distributions obtained differ substantially from those found in other experiments aimed directly at determining these distributions.

An example illustrating the first procedure mentioned above is shown in fig. 6b. The dot-dashed lines plotted in this figure for ΔQ_v , ΔR_v , and ΔC_v were calculated from optical-model potential wells generated by first assuming a fairly realistic density distribution given by

$$\begin{aligned} R_\rho &= 1.16A^{\frac{1}{3}} \text{ fm}, \\ b_\rho &= 1.0 \text{ fm}, \end{aligned} \quad (30)$$

and folding in a Gaussian interaction of the form

$$f_G(r) = -V \exp [-(r/a_G)^2], \quad (31)$$

with a range $a_G = 1.86$ fm chosen so the experimental values of Q_v are reproduced. The width b_c of this interaction is 1.32 fm, since

$$b_c = a_G/\sqrt{2}. \quad (32)$$

The long-range part of the Hamada-Johnston potential, which is currently in vogue for the interpretation of proton-nucleus scattering data [see the discussion in refs. ¹⁴) and ¹⁵)], has a width of about 1.4 fm and is quite similar to the interaction used here.

Eq. (17) shows that the surface width b_v of the potentials resulting when (31) is folded into (30) is 1.65 fm. This is not a very satisfactory result since it is substantially larger than the 1.3 fm value obtained by simply fitting Woods-Saxon wells to experiment.

It should be pointed out in passing that if the potentials being considered in fig. 6b were leptodermous, ΔQ_v and ΔC_v would lie on the thin straight lines predicted by eqs. (12) and ΔR_v would be exactly zero. The reason the dot-dashed lines representing these quantities deviate is that the long range of the folding interaction produces potential wells so diffuse that they are no longer leptodermous for the smaller nuclei.

The other possible approach to the problem of generating optical potentials by folding is to vary both the radius of the density distribution and the range of the force. [An extensive analysis of this type is contained in ref. ⁴)]. When this is done the optical-model wells obtained have geometrical properties similar to those obtained by fitting Woods-Saxon wells [see eq. (29)]. Since $b_v \approx 1.3$ we can see from eq. (17) that b_c must be approximately 0.83 fm, which corresponds to a range $a_G = 1.17$ fm for a Gaussian interaction. Since $R_\rho = R_v$ [from eqs. (20)] it is clear [from eq. (29)] that this fitting procedure must result in density distributions for which

$$R_p \approx 1.16A^{\frac{1}{3}} + 0.45 \text{ fm}, \quad (33)$$

in substantial disagreement with what is known about this quantity. Unreasonably large density distributions are always obtained when this procedure is employed, simply because of the geometrical relations involved.

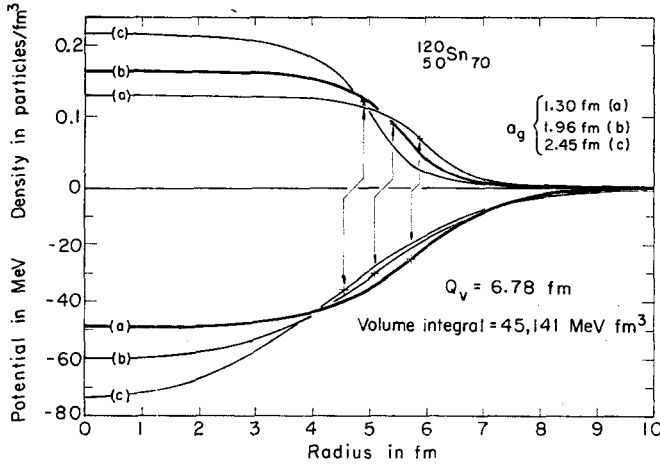


Fig. 7. Sample density distributions and corresponding potential wells for $^{120}_{50}\text{Sn}_{70}$ are plotted against the radial distance. In each of the three cases shown the potential is generated by folding eq. (31), a non-saturating force, into the density with force parameters chosen so as to give the same values for Q_v and the volume integral of the potential. For case (a) the potential corresponds to experiment. For case (b) the density corresponds to experiment. The thin lines connect half-value points to show that this quantity is always smaller for the potential.

Fig. 7 serves to further illustrate the points developed above. In this figure the nuclear density distribution for $^{120}_{50}\text{Sn}_{70}$ and the potential well related to it by folding in a Gaussian interaction are plotted for three different cases. For the case (a) an unrealistically extended density distribution was chosen so that the optical-model well would have the geometric properties

$$\begin{aligned} C_v &= 5.76 \text{ fm}, \\ b_v &= 1.35 \text{ fm}, \end{aligned} \quad (34)$$

determined by fitting to experiment¹¹). For case (b) the density distribution was chosen to correspond to experiment, and a long-ranged folding interaction was chosen so as to reproduce the equivalent rms radius Q_v and volume integral of the experimentally determined potential. This requires a longer-range interaction and results in a potential well considerably more diffuse than that determined by fitting directly to experiment. If [as in case (c)] an even smaller density distribution is employed, an even longer range interaction is required to maintain the value of Q_v , and an extremely diffuse potential results.

Another interesting aspect of fig. 7, which serves to confirm eq. (20), is that C_v is less than C_ρ (corresponding points are indicated by crosses and connected by a line in the figure) by an amount which increases as the range of the folding interaction increases. This means that if such densities and potentials (related by a simple folding) were both to be represented by Fermi distributions the radius parameter c of the Fermi distribution representing the potential would always have to have a substantially smaller value than the value for c for the corresponding density distribution. [Recall that $C = R_{\frac{1}{2}} = c$ according to eq. (70).]

4.3. DENSITY-DEPENDENT INTERACTIONS

It might have been anticipated that nuclear density distributions and optical-model potential wells are not related in a way corresponding to the folding in of a simple two-body interaction such as the one given in eq. (31). If any sort of self-consistent calculation of nuclear properties is attempted with such a force the system collapses. It is well known that the force employed in such calculations must become effectively weaker as the nuclear density increases so as to lead to saturation. This feature (the apparent decrease in interaction strength with increasing density) is just the feature needed to resolve the difficulties encountered in the optical-model fits. Fig. 8 shows the relationship between the density distribution of $^{208}_{82}\text{Pb}_{126}$ and an optical-model potential well obtained by folding in a saturating two-body interaction. The form of the interaction chosen for this example was

$$f_c(r) = -V e^{-(r/a)^2} (1 - c\rho^3), \quad (35)$$

where

$$V = 51 \text{ MeV}, \quad a = 1.39 \text{ fm}, \quad c = 2 \text{ fm}^3. \quad (36)$$

In fig. 8 the neutron and proton density distributions predicted by the droplet model are shown. Their equivalent sharp radii are indicated by short vertical bars. The equivalent sharp radius of the density R_ρ (the sum of R_n and R_z) is shown as a long vertical line. As we know from eq. (19) the equivalent sharp radii are identical for the density and the potential generated from it with a simple interaction. Consequently, the same vertical line that locates R_ρ also serves to locate R_v in the case (shown as the lower dashed line in the figure) where the interaction of eq. (35) is employed without the last factor. When we consider the solid curve where the entire interaction is used, including the last term with its density dependence, we see that the discrepancy that mars earlier attempts to relate experimentally determined densities and potential wells has disappeared. The solid curve labeled V in fig. 8 approaches its bulk value more quickly than does the dashed curve, because the interaction generating it becomes effectively weaker towards the interior. Consequently, the equivalent sharp radius R_v of this potential well lies outside of R_ρ , in agreement with experiment.

Since the potential well produced by the saturating interaction, eq. (35), is shallower everywhere than the corresponding potential well produced by the non-saturating part of the interaction it is possible to gain the impression from fig. 8 that the non-

saturating potential is larger (in some vague sense), even though the geometric fact is the reverse. To offset this illusion the dashed curve representing the non-saturating part of the interaction has been replotted as a second dashed curve having the same bulk value as the solid curve representing the potential produced by the complete interaction. In comparing these two curves (with the same bulk values) it is easier to see that the equivalent sharp radius R_v of the saturating potential lies 0.5 fm outside that of the non-saturating potential. Indeed, it is possible, in analogy with the proof of eq. (19), to establish the theorem that the equivalent sharp radius R_v of any potential well produced by a saturating interaction (i.e., the strength decreases with increasing density) is larger than that for a potential well produced by the non-saturating part of the same interaction.

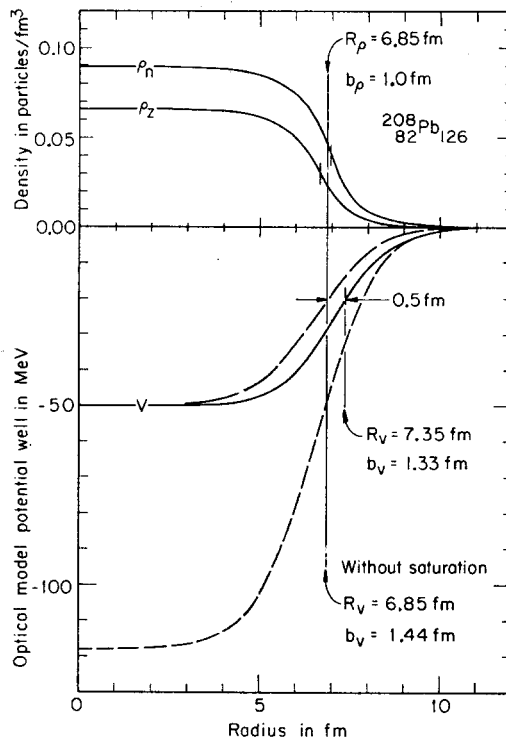


Fig. 8. Droplet model density distributions for $^{208}_{82}\text{Pb}_{126}$ are plotted against radial distance in the upper part of the figure. Short vertical bars on ρ_n and ρ_p indicate the location of the equivalent sharp radii R_n and R_p . The long vertical line indicates the location of the equivalent sharp radius of the total density R_ρ . This same line indicates the location of the equivalent sharp radius of the potential (obtained by folding the non-saturating part of eq. (35) into the density) plotted in the lower part of the figure as a dashed line. The lower dashed line is the potential itself and the upper dashed line is the same curve normalized to the solid line which represents the potential obtained when the complete saturating interaction, eq. (35), is used. A shorter vertical line indicates the location of the equivalent sharp radius of this latter potential and shows that it lies substantially outside that of the non-saturating potential.

It is necessary to refer back to fig. 6 in order to see how the use of a saturating interaction improves the agreement with experimentally determined optical-model potential wells throughout the periodic table. In fig. 6c the dot-dashed lines represent the geometrical properties of the potentials obtained by folding the saturating interaction of eq. (35) into the density distributions predicted by the droplet model. Contrast the good agreement thus obtained with the rather poor agreement obtained in fig. 6b with the use of a non-saturating interaction.

The functional form of the density dependence used in eq. (35) is suggested by various considerations. In the Thomas-Fermi (or WKB) approximation, the Fermi-momentum – and hence the average momentum – of the target nucleons is proportional to $\rho^{\frac{1}{3}}$. The effective two-body interaction is expected to be an even function of the relative momentum, and the leading term (quadratic in momentum or proportional to $\rho^{\frac{2}{3}}$) in a power series expansion may be sufficient. Many different phenomenological interactions having either this form or a closely related one have found application in Thomas-Fermi calculations^{5, 16}), Hartree-Fock calculations^{17, 18}), and in studies of the optical model itself^{14, 19, 20}).

No special effort has been made to refine the choice of effective two-body interaction used here, since the main concern is with the purely geometrical aspects of the problem. In a more general study of the relation between optical-model wells and nuclear properties, the energy and isospin dependence of the effective interaction would have to be considered, as well as effects due to antisymmetrization.

Slanina and McManus¹⁴) have considered a density-dependent interaction due to Green²¹) that is similar to the one used here with a slightly weaker density dependence. The potential was folded into empirical density distributions in an attempt to construct potentials similar to those found in optical-model fits. They noted the improved agreement obtained by including a density dependence in the interaction.

Another point that must be mentioned is that the experimental optical-model wells are not unique. The wells we have considered here correspond to approximately the same energy, but one would expect different geometrical properties (as well as potential strengths) for different energies. In addition, the way in which the imaginary potential is included (whether proportional to the real potential or to its derivative) also influences the outcome of a standard optical-model fit. Consequently, the parameters in the saturating interaction eq. (35) would have to be made energy dependent and dependent in some way on the geometry of the imaginary potential if one wished to have a single interaction that would apply to all cases.

What we have shown is that nuclear density distributions and potential wells that have been deduced from experiment *cannot* be related satisfactorily by folding in a simple non-saturating two-body interaction for purely geometrical reasons. It is likely that any number of reasonable saturating interactions will be able to provide this connection whether they be non-local, density dependent, or velocity dependent.

It should be noted in passing, that objections to potentials generated by folding a simple non-saturating two-body interaction into the density, and the obvious incon-

sistencies that arise when this is attempted, are much more difficult to recognize for the light elements. The density distributions of these nuclei and their optical-model potential wells are no longer leptodermous (indeed, they might be called holodermous since they are better represented by Gaussian functions than by Fermi functions); consequently, many of the geometric relations employed in the preceding discussion are no longer applicable. Of course, analogous relations can be derived for these distributions and an analysis carried out similar to what has been done here, but the interpretation is not as easily accomplished.

5. Summary

A set of geometrical relations has been presented, based on a study by Süssmann²⁾, that relate various properties of leptodermous distributions. These relations were applied to the experimental information available on nuclear density distributions. The results obtained from different experiments were shown to be consistent and (with the help of the droplet model) to lead to a value of r_0 , the radius constant of standard nuclear matter, of $1.16 \text{ fm} \pm 1\frac{1}{2} \%$.

The same geometrical relations that were applied to the density distributions were then applied to the optical-model potential wells for nuclei throughout the periodic table. It was shown that the experimental densities and potentials cannot be related satisfactorily by a simple two-body interaction unless the force includes features expected from nuclear saturation.

The main purpose of this work has been to point out the existence of certain relations between geometrical properties of nuclei and the pitfalls encountered when these are ignored.

This work has benefitted greatly from discussions the author has had over the years with W. J. Swiatecki. It was stimulated by encounters with Robert Hofstadter, Daphne Jackson, D. G. Ravenhall, and Fred Becchetti. Specific contributions were made by Georg Süssmann and Fred Petrovich.

References

- 1) H. R. Collard, L. R. B. Elton and R. Hofstadter, in Nuclear radii, vol. 2, group I, Landolt-Börnstein, Numerical data and functional relationships in science and technology (Springer-Verlag, Berlin, 1967)
- 2) G. Süssmann, unpublished draft of Lawrence Berkeley Laboratory Report LBL-1615
- 3) K. W. Ford and John G. Wills, Phys. Rev. **185** (1969) 1429
- 4) G. W. Greenless, G. J. Pyle and Y. C. Tang, Phys. Rev. **171** (1968) 1115
- 5) W. D. Myers and W. J. Swiatecki, Ann. of Phys. **55** (1969) 395
- 6) W. D. Myers, Phys. Lett. **30B** (1969) 451
- 7) W. D. Myers, Nucl. Phys. **A145** (1970) 387
- 8) A. S. Tyapin, Yad. Fiz. **1** (1965) 581 [Engl. transl.: Sov. J. Nucl. Phys. **1** (1965) 416]
- 9) A. R. Bodmer, Nucl. Phys. **17** (1960) 388
- 10) L. R. B. Elton, Nuclear sizes (Oxford, 1961)

- 11) B. Hahn, D. G. Ravenhall and R. Hofstadter, Phys. Rev. **101** (1956) 1131
- 12) M. P. Fricke, E. E. Gross, B. J. Morton and A. Zucker, Phys. Rev. **156** (1967) 1207
- 13) C. B. Fulmer, J. B. Ball, A. Scott and M. L. Whiten, Phys. Rev. **181** (1969) 1565
- 14) D. Slanina and H. McManus, Nucl. Phys. **A116** (1968) 271;
D. Slanina, Ph.D. thesis, Michigan State University, 1969, unpublished
- 15) L. G. Owen and G. R. Satchler, Phys. Rev. Lett. **25** (1970) 1720;
G. R. Satchler, Comm. Nucl. Particle Phys. **5** (1972) 39
- 16) L. Wilets, Phys. Rev. **101** (1956) 1805
- 17) C. B. Dover and Nguyen Van Giai, Nucl. Phys. **A190** (1972) 373
- 18) J. W. Negele, Phys. Rev. **C1** (1970) 1260
- 19) F. G. Perey, Phys. Rev. **131** (1963) 745
- 20) A. E. S. Green, T. Sawada and D. S. Saxon, The nuclear independent particle model (Academic Press, New York, 1968)
- 21) A. M. Green, Phys. Lett. **24B** (1967) 384